Growth, Spectral, Quantum Chemical and Biological Investigations on 2-amino-6-methylpyridinium-4-hydroxybenzoate

L.Chandra [1] ,J.Chandra Sekaran [2], K.Perumal [2]

[1] Department of Physics, Chikkaiah Naicker College, Erode-638004, Tamilnadu, India

[2] Department of Physics, Sri Ramakrishna Mission Vidyala College of Arts and Science,

Coimbatore-641020, Tamilnadu, India

Abstract:

In the present work, 2 amino 6 methylpyridine is mixed with 4 hydroxy benzoic acid in the molar ratio of 1:1 using methanol as solvent and 2A6M4H was crystallised at room temperature. The presence of electron donor and electron acceptor groups at the opposite ends of conjugated π electron structure has increased the nonlinear optical activity of the as grown sample .The as grown single crystal is subjected to structural, spectroscopic, thermal and biological studies and the results are investigated.

Key words*: 2A6M4H, conjugated π electron*.

1. Introduction

Nowadays these SHG and THG active materials have been of great interest due to their potential applications in the field of telecommunications, THz wave generation, electro-optic modulator, photonic devices, optical data storage and medical diagnostics [1-5]. Also, organic materials are emerging as an alternative to inorganic materials. Because the electronic susceptibility ($\chi^{(2)}$) of the organic NLO materials is in several orders of higher magnitude than that of the inorganic materials. Besides, more effect was put towards the growth of organic materials due to their higher molecular polarizability (β) and higher laser damage threshold, fast and large nonlinear optical response over a broad frequency range, large electro-optic coefficient, lower value of dielectric constant and greater ease of device fabrication and offers flexibility of molecular design via the proper synthetic method [6-9]. Organic molecules substituted with an electron donor and electron acceptor groups at the opposite end of a conjugated π-electron system exhibit higher nonlinear optical activity [10-12]. Organic molecules with significant nonlinear optical activity generally consist of conjugated π-electron structure. The conjugation π-electron moiety gives a path for the whole length of conjugation under the perturbation of an external electric field. Functionalization of both ends of the π bond systems with an appropriate electron donor and acceptor groups can increase the asymmetric electronic distribution in both the ground and excited states and thereby increase the optical nonlinearity [13, 14].

Motivated by these facts for the first time in literature, 2-amino-6-methylpyridine was mixed with 4-hydroxybenzoic acid in the present work to grow the crystals. The grown crystals were subjected to various characterization techniques such as single crystal/powder XRD, UV, FTIR, TG/DTA and Z-scan studies.

1. 2. Experimental

1.2.1. Crystal growth

The 2-amino-6-methylpyridinium-4-hydroxybenzoate (2A64H) was synthesized using commercially available high purity 2-amino-6-methylpyridine and 4-hydroxybenzoic acid. They were mixed in a stoichiometric ratio of 1:1 in methanol and stirred continuously for about half an hour using a magnetic stirrer. To remove the unwanted impurities this solution was filtered using Whatman filter paper and transferred into a crystallizing vessel. The top of the beaker was enclosed with a perforated thin polythene sheet. Finally, the solution was left undisturbed for crystal growth. After a span of about 9 days, good quality single crystals of 2A64H were harvested. **Fig.1**. is the photograph of the grown crystals.

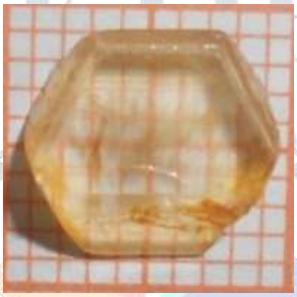

Fig. 1. As grown crystals of 2A6M4H.

1.3 Results and Discussion

1.3.1 XRD Analysis

From the single crystal XRD results, it was found that the 2A6M4H crystallized in monoclinic crystal system with a centrosymmetric space group of $P2_1/c$. The obtained unit cell dimensions were a = 11.9487 (3) Å, b = 9.2950 (3) Å, c = 12.4062 (3) Å, β= 117.116 (2)°, V = 1226.49 (6) $Å^3$, Z = 4, and they agreed well with the earlier data [19]. The powder XRD spectrum of 2A6M4H was carried out using the RICH SIEFERT X-ray powder diffractometer equipped with CuKα radiation at a wavelength λ = 1.5405 Å and detected by using a scintillation counter. The spectrum was recorded at room temperature and scanned over the 2θ range of 10-60°. The title compound was crushed into fine powder and subjected to the PXRD analysis. The various planes (hkl) in the diffractogram were indexed using the TREOR 90 programme. An intense and sharp peak diffractogram implies the crystalline nature of the compound.

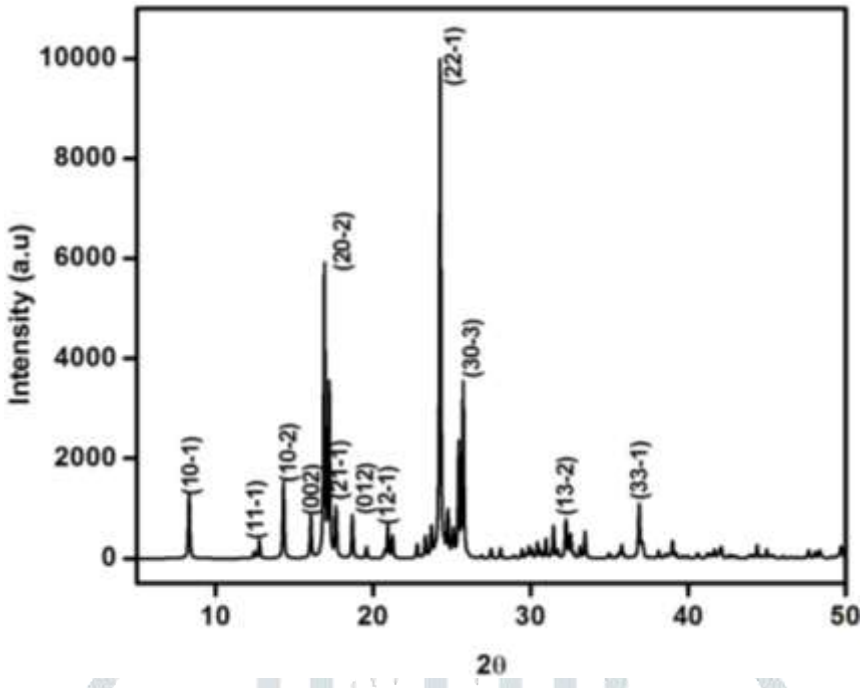

Fig. 2. Powder XRD spectrum of 2A6M4H.

1.3.2 FTIR analysis

The formation of the charge transfer complex is strongly evidenced by the presence of the main characteristics infra-red bands of the donor and acceptor molecules in the spectrum with slight changes in frequencies. The well assignment of the bands, observed in the vibrational spectra is an indispensable step in solving the structural problems of any molecule. The IR spectrum of 2-amino 6-methylpyridinium 4-hydroxybenzoate in the region 4000–400 cm^{-1} is shown graphically in **Fig 3**. The absorption bands at 2790 and 2679 cm^{-1} have been assigned to aromatic C–H stretching vibration of the complex. The bands at 1278 and 1244 cm^{-1} are due to CN stretching of vibration. The symmetric and asymmetric stretching modes of the COO− group are revealed by peaks at 1592 $cm^{-1}$and 1529 cm^{-1} respectively. The NH and OH bending vibrations were observed at 1664, 1642, 993 and 945 cm^{-1} respectively. The absorptions at 851 and 1050 cm^{-1} are assigned to aromatic NH wagging vibration. The vibrations at 1356 cm^{-1} and 730 owe to CH bending and CH rocking vibration. The aromatic C-C vibration appears at 1909 and 1495 cm^{-1}. The bands at 694 and 617 cm^{-1} is due to NH out-of-plane bending and OH out of plane deformation. The carboxylic C-O stretching vibrations were observed at 1165 and 1135 cm^{-1}. The vibration at 779 cm-1 is assigned to the COO– scissoring vibration.

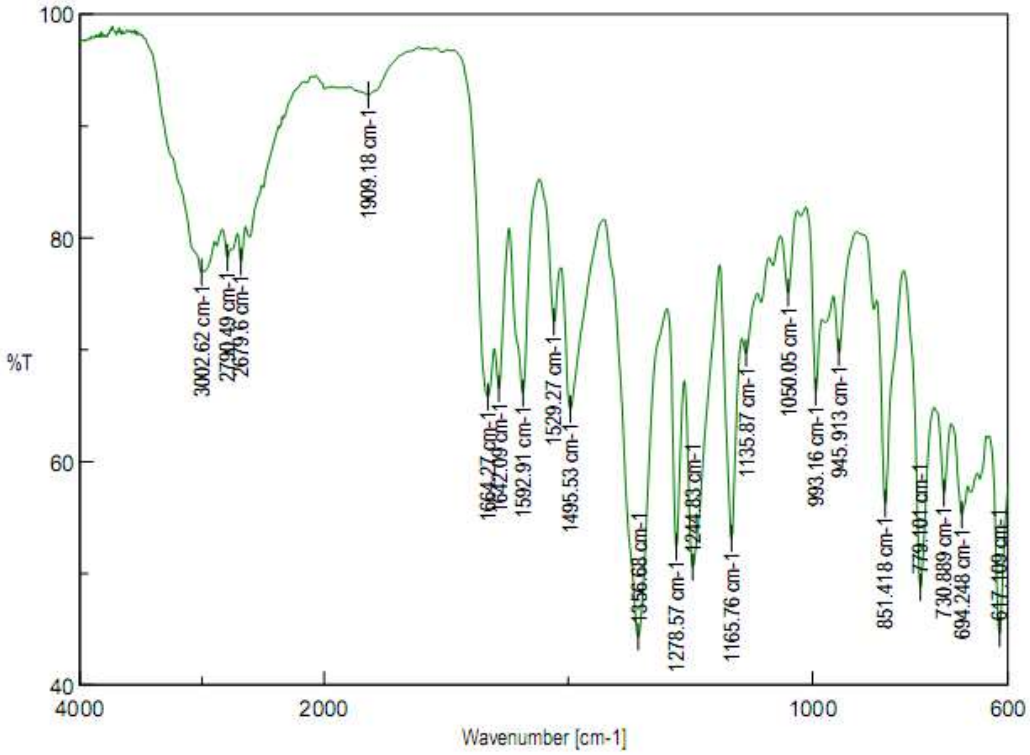

Fig.3. FTIR spectrum of 2A6M4H.

1.3.3 Optical Studies

In order to study linear optical characteristics, grown crystals of 2A6M4H with a thickness of about 2 mm were subjected to UV-Vis-NIR spectral analysis in the wavelength range from 200 to 1200 nm, using Varian Cary UV-Vis-NIR spectrophotometer is shown in **Fig.4**. In NLO crystalline compounds, improved optical transmittance is one of the most important properties. Owing to an occurrence of absorption peaks in between shorter to longer wavelength region in a material, a conversion efficiency of wavelength get altered. Hence it is essential to monitor absorptions in the above-said range. From the spectrum (**Fig. 4**), it is clear that UV cut-off wavelength of the grown 2A6M4H crystal was noted at 353 nm. The crystal is entirely transparent beyond cut-off wavelength up to 1200 nm. Due to the electronic transition between 'non-bonding' n orbital and anti-bonding π orbital represented as π*, strong absorption peak has taken place around 353 nm [3]. Moreover, transparent character of the crystal is suitable and a prerequisite for second and third harmonic lights with wavelengths (λ = 532 nm) and (λ = 354.6 nm) respectively originated from Nd: YAG laser with laser light wavelength (λ = 1,064 nm) . The optical absorption co-efficient (α) of grown 2A6M4H crystal was obtained from the following relation

$$\alpha = \frac{2.303 \log (1/T)}{d} \qquad (1)$$

Where,

d is the thickness of the crystal and

T is the transmittance.

The absorption co-efficient (α) of 2A6M4H was determined using the following relation.

$$(\alpha h\nu) = A\,(h\nu - E_g)^n \qquad (2)$$

Where A is constant. 'h' is Planck's constant and ν is frequency of incident photons. The above equation is well suitable for an allowable direct transition between the simple parabolic bands. The optical energy gap (E_g) of 2A6M4H is calculated using Tauc's plot of $h\nu$ versus $(\alpha h\nu)^{1/n}$, by extrapolating the linear portion of the curve near the start of absorption edge towards the energy axis is shown in **Fig. 5.** The band gap value of 2A6M4H crystal was estimated at 3.61 eV. The wide band gap of this crystal shows the large transmittance in the visible region.

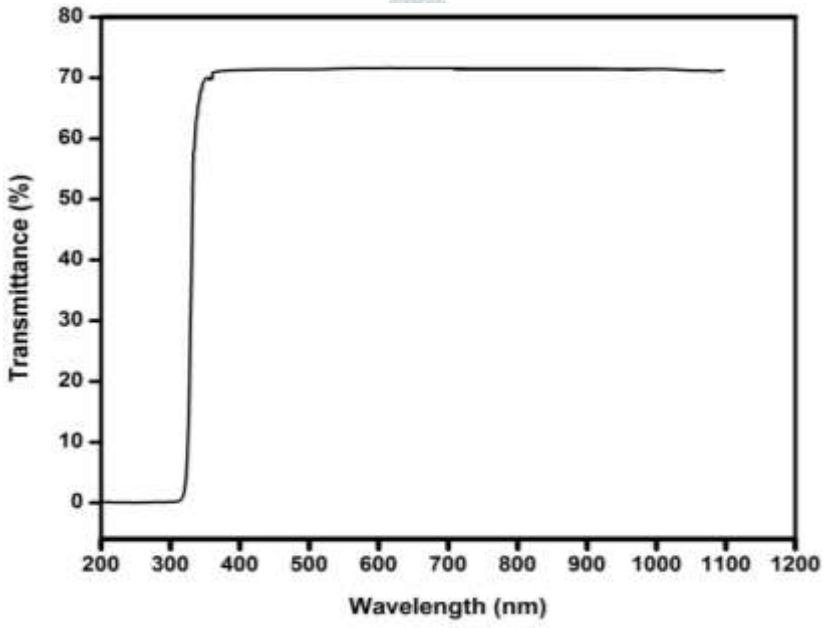

Fig. 4. Optical transmission spectrum of 2A6M4H

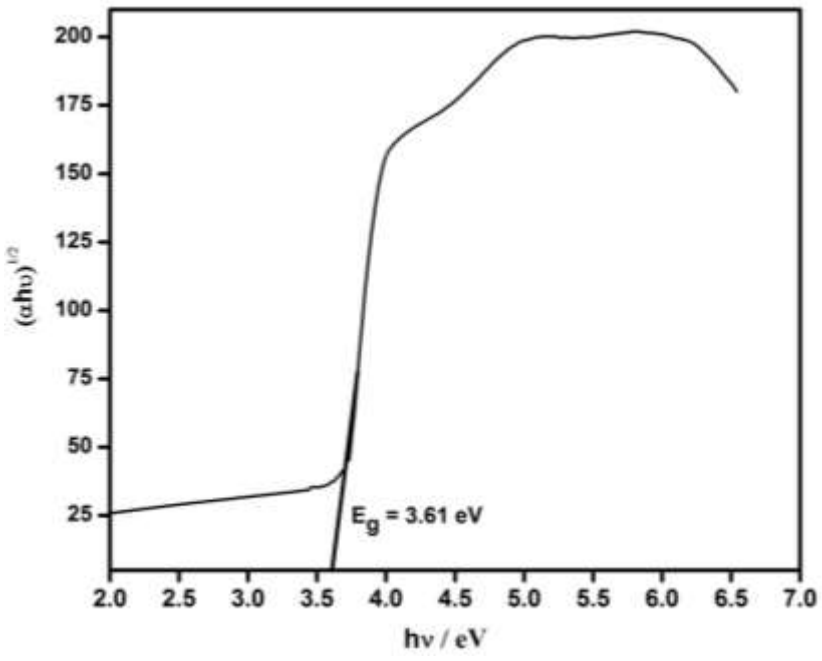

Fig. 5. Tauc's Plot of 2A6M4H.

1.3.4 TG/DTA studies

The simultaneous TG–DTA was performed on 8.943 mg powder sample of 2A6M4H which was derived from its single crystals, and the resultant curves are shown in **Fig. 6**. The DTA curve shows an endothermic peak at 127 °C, where the melting begins. The second endothermic peak at temperature 154.09 °C corresponds to the end of melting and starting of decomposition. The third endothermic peak at 224.4 °C indicates further decomposition. The sharpness of the endothermic peak shows a good degree of crystallinity of the grown crystal. The absence of lattice-entrapped crystallization solvent or impurity is confirmed by the absence of mass loss up to 127 °C. The shape of the TG curve after the melting point represents the thermal decomposition of 2A6M4H with the formation of volatile reaction products. The decomposition occurs with two stages. In first stage, mass loss about 11 % occurs between 149.51 and 183 °C. This mass loss may be attributed to the formation of volatile substances such as carbon monoxide and NH_2. The second-stage mass loss starts at 154.09 °C, and it continues up to about 243 °C. This mass loss could be attributed to the decomposition of CO_2,CH_3, and remaining moiety and also the removal of almost all fragments as gaseous products. Since there are no exothermic or endothermic transitions below the melting point of the sample, the material is moisture free and stable up to 127 °C. The melting point of 2A6M4H obtained by melting point apparatus was found to be 153.12 °C. All these observations on 2A6M4H showed that it could be useful for fabricating NLO devices below 127 °C

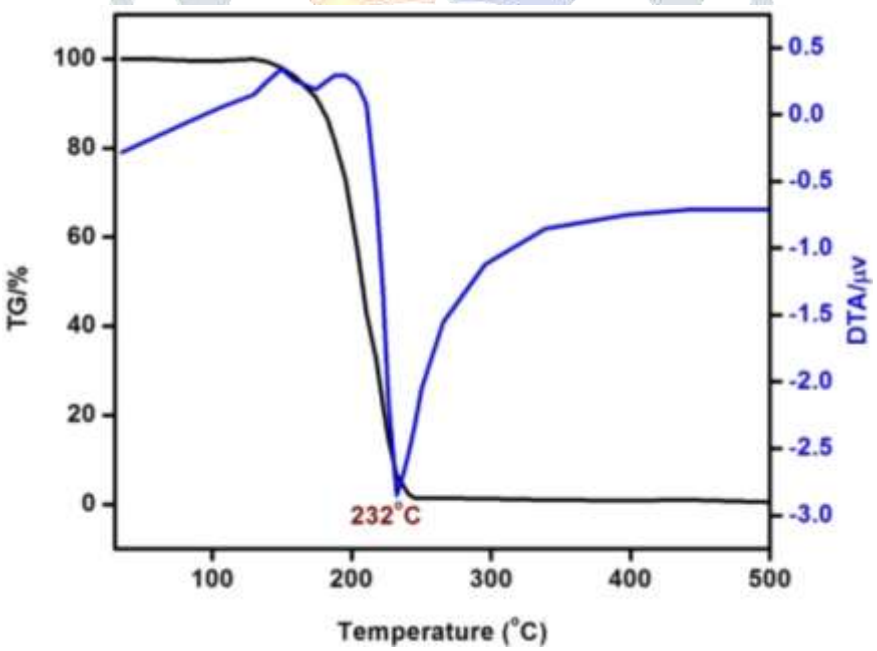

Fig. 6. TG/DTA spectrum of 2A6M4H.

1.3.5 Dielectric studies

Dielectric studies for the grown crystals were studied using HIOKI LCR HITESTER (Model 3532-50). Measurements were carried out at the temperature ranging from 303K to 335K. Crystals were placed between two copper plates and thus parallel capacitance was made for the measurement. The capacitance of the crystal was measured by varying the frequency range 50Hz to 5MHz. The dielectric constant of the crystal was calculated using the obtained capacitance values by the given formula

$$\varepsilon_r = \frac{Cd}{\varepsilon_o A} \qquad (3)$$

Where C is the measured capacitance, d is the thickness of the crystal, A is the cross-sectional area of the crystal and ε_o is the free space permittivity of the crystal. **Fig. 7(a)** shows dielectric constant Vs frequency for the grown crystal. From the figure, it is concluded that dielectric constant is very high at low frequency and also it increases with increase in temperature. As the frequency increases dielectric constant value decreases and attains a constant value at very high frequency. Dielectric studies provide useful information concerning dielectric constant thus arises from different polarizations namely electronic, ionic, space charge and orientation. In these polarizations, space charge polarization will reckon on the perfection and purity of the sample. So in the present system, it is active at low frequency region and high temperature [16-18]. **Fig. 7(b)** shows frequency dependent dielectric loss for the grown crystal. The dielectric loss is very low at high frequency. This low value indicates crystals own good quality with lesser defects which make it a suitable candidate for optoelectronic applications [19, 20].

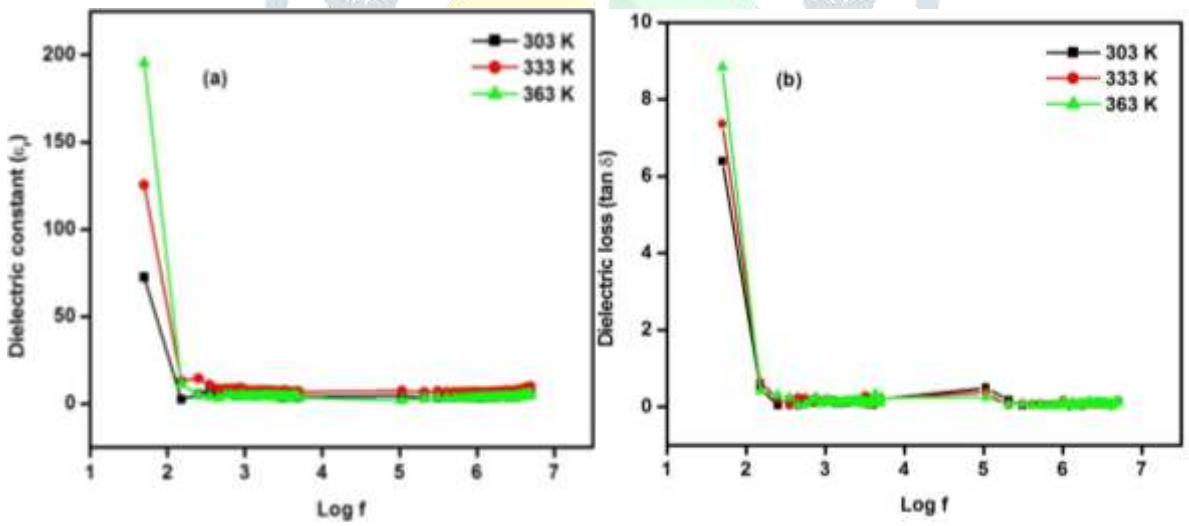

Fig. 7 (a) Dielectric constant versus frequency of 2A6M4H crystal

7**(b)** Dielectric loss versus frequency of 2A6M4H crystal

1.3.6 Photoconductivity

Photoconductivity measurements for grown 2A6M4H crystals were taken using Keithley electrometer (Model 6517B). Dark and photocurrent measurements on these crystals were carried out by two-probe technique at room temperature. Parallel faces of the crystals were coated with electronic grade

silver paint and a small copper wire was fixed both sides of the samples. The sample was then connected in series to a DC power supply and electrometer. For dark current measurements sample was protected from all the radiations and the input applied voltage was increased from 10V to 100V in steps of 10V. The corresponding dark current was recorded. For photocurrent measurements, illumination from 100W halogen lamp containing iodine vapour and tungsten filament was used. **Fig. 8** depicts the dark current and photocurrent response for 2A6M4H crystal. From the figure, it is accomplished that dark and photocurrents are linear with applied input voltage and the dark current is higher than photocurrent which is termed as negative photoconductivity. It may be due to the decrease of charge carriers in the presence of illumination. Materials with negative photoconductivity can be used for UV and IR detector applications [21].

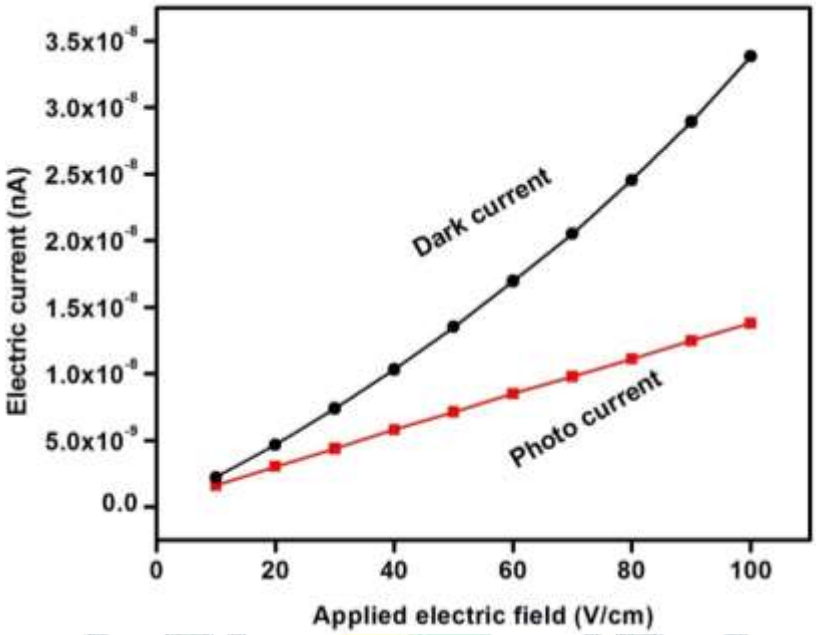

Fig. 8. Photoconductivity response of 2A6M4H crystal.

1.3.7 Z-Scan studies

The Z-scan is a well-known experimental technique to measure the intensity dependent third order nonlinear susceptibility of the materials [22, 23]. The open and closed aperture Z-scan configurations are used to investigate the nonlinear absorption coefficient β and nonlinear refractive index n_2. **Fig 9(a)** shows the normalized transmittance (T) with a closed aperture as a function of the distance z along the lens axis in the far field. The **Fig 9(b)** shows the normalized transmittance with an open aperture as a function of the distance z along the lens axis in the far field. The nonlinear refractive index (n_2) and nonlinear absorption coefficient (β) are given by,

$$n_2 = \frac{\Delta\phi}{kI_0L_{eff}} \qquad (4)$$

$$\beta = \frac{2\sqrt{2}\,\Delta T}{I_0L_{eff}} \qquad (5)$$

where k is the wave number $k = 2\pi/\lambda$ and

$$L_{eff} = \frac{1-e^{(-\alpha L)}}{\alpha} \quad (6)$$

with $I_o = \frac{P}{\pi\omega_0^2}$ defined as the peak intensity within the sample, where L_{eff} is the thickness of the sample and α is the linear absorption coefficient. The real and imaginary parts of the third-order nonlinear susceptibility χ(3) are defined as

$$Re\chi^{(3)} = 10^{-4}\frac{(\varepsilon_o C^2 n_o^2 n^2)}{\pi}(esu) \quad (7)$$

$$Im\chi^{(3)} = 10^{-2}\frac{(\varepsilon_o C^2 n_o^2 \lambda\beta)}{4\pi^2}(esu) \quad (8)$$

where ε_0 is the vacuum permittivity, n_0 is the linear refractive index of the sample and c is the velocity of light in vacuum. Thus, we can easily obtain the absolute value of χ(3) using the following formula

$$\left|\chi^{(3)}\right| = [(Re\chi^{(3)})^2 + (Im\chi^{(3)})^2]^{\frac{1}{2}} \quad (9)$$

As seen from the closed aperture Z-scan curve, the prefocal transmittance valley is followed by the post focal peak, which is the positive nonlinearity. The calculated value of the nonlinear refractive index (n_2) is 6.40149 10^{-8} cm^2/W. The value of the nonlinear absorption coefficient (β) estimated from the open aperture Z-scan curve is 2.4603 x 10^{-4} cm/W. The third order susceptibility of 2A6M4H is 1.3061 x 10^{-7} esu. As the material has a positive refractive index, it results in self-focusing nature of the material, which is an essential property for all optical limiting devices [3].

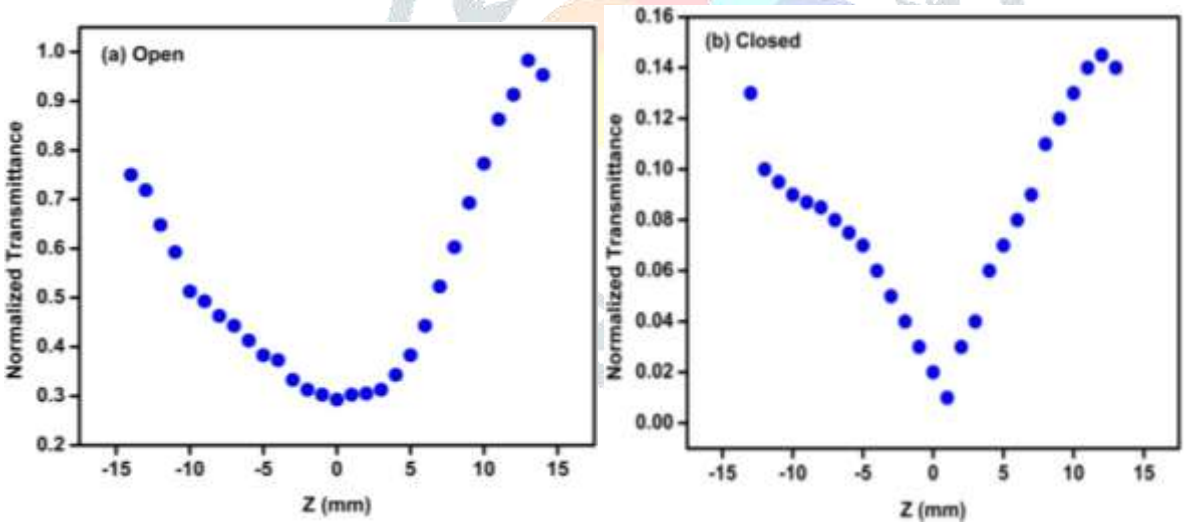

Fig. 9 (a) Normalized transmittance with open aperture as a function of Z position

9 (b) Normalized transmittance with closed aperture as a function of Z position

1.3.8 FMO analysis

The excitation energies of the neutral system can be calculated by the energy difference between the highest occupied molecular orbital (HOMO) and the lowest unoccupied molecular orbital (LUMO). The HOMO is the outermost orbital that primarily acts as an electron donor and directly related to the ionization

potential, whereas the LUMO is the innermost orbital that largely acts as the electron acceptor and directly related to the electron affinity. The conjugated molecules are characterized by HOMO and LUMO separation, which is the result of a significant degree of intermolecular charge transfer (ICT) from the electron–donor to the efficient electron–acceptor group. The energy gap between HOMO and LUMO characterizes the properties such as optical polarizability. The HOMO–LUMO energy gap of the title compound has been calculated at the B3LYP/6–311+G basis set. The topologies of HOMO and LUMO orbitals of 2A6M4H are shown in **Fig 10**. From the figure, it could be observed that HOMO is delocalized over the nitro group and phenyl ring attached to the 4-hydroxybenzoate anion. By contrast, the LUMO is delocalized over entire 2-amino 6-methylpyridinium cation. It could also be observed that the 2A6M4H exhibit the charge transfer between 4-hydroxybenzoate anion 2-amino-6-methylpyridine cation.

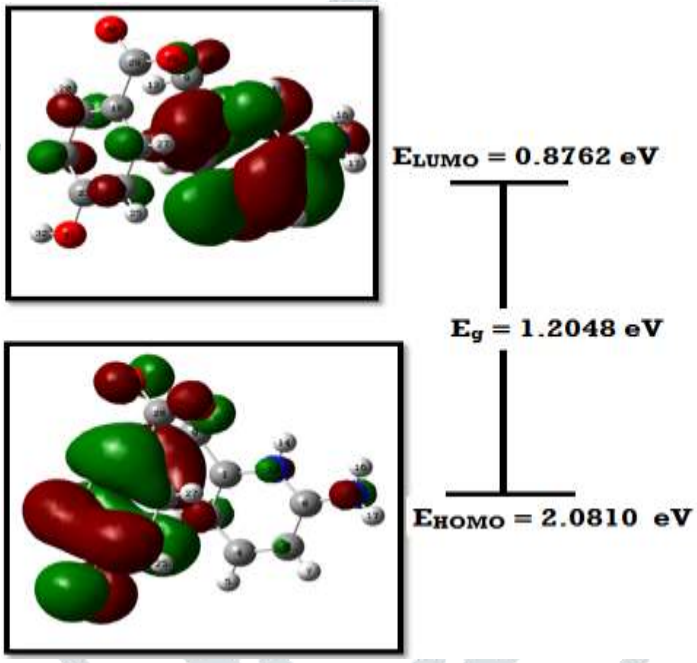

Fig. 10. The atomic orbital compositions of the frontier molecular orbital for 2A6M4H.

1.3.9 Antioxidant studies

The free radical scavenging ability of the synthesized compound with DPPH and H_2O_2 radical is studied in this analysis. The ascorbic acid is used as standard complex for comparison of results. **Fig. 11** represents IC_{50} values of the tested compound. The result confirms that the synthesized compound can reduce the concentration of the initial free DPPH and H_2O_2 radicals.

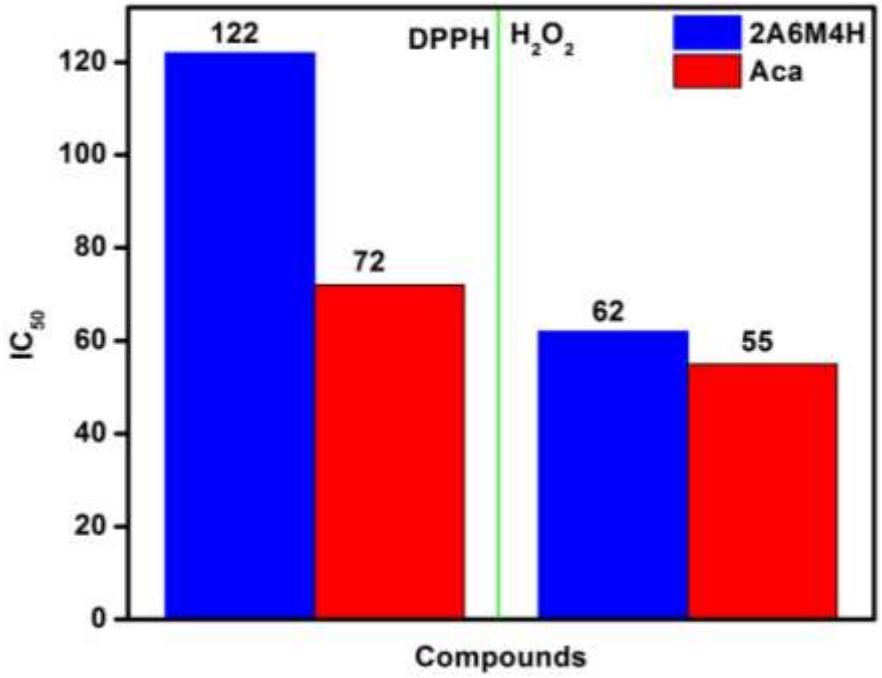

Fig. 11. DPPH and H_2O_2 radical scavenging ability of 2A6M4H.

1.4 Summary

The single crystals of 2-amino-6-methylpyridinium-4-hydroxybenzoate were grown successfully by slow evaporation technique at room temperature. The centrosymmetric space group and structure of the grown crystal were confirmed by the single crystal XRD analysis. The presence of various functional groups in crystal was analyzed by The FTIR spectrum. UV-Vis absorption analysis showed the transparency of the crystal beyond 400 nm wavelength (visible) region which is a desired property for various NLO applications. From the transmittance value, the optical band gap was calculated for the grown crystals. The characteristic of low dielectric loss at high frequencies for grown crystals suggested that the grown crystals possessed enhanced optical quality with lesser defects. The HOMO-LUMO energy for the compound was determined. The self-focusing nature of the crystal was analysed by the Z-scan study. The antioxidant activity confirmed that the charge transfer complex can serve as a possible antioxidant against DPPH radical.

References

[1] A. Majchrowski, I.V. Kityk, T. Łukasiewicz, A. Mefleh, S. Benet, Opt. Mater. **15** (2000) 51-58.

[2] P. Pandi, G. Peramaiyan, S. Sudhahar, G. Chakkaravarthi, R. Mohan Kumar, G. Bhagavannarayana, R. Jayavel, Spectrochim. Acta Part A **98** (2012) 7–13

[3] K. Thirupugalmani, S. Karthick, G. Shanmugam, V. Kannan, B. Sridhar, K. Nehru, S. Brahadeeswaran, Optical Materials **49** (2015) 158-170.

[4] R.P. Jebin, T. Suthan, N.P. Rajesh, G. Vinitha, U. Madhusoodhanan, Spectrochim. Acta Part A **135** (2015) 959-964.

[5] A. Silambarasan, M. Krishna Kumar, A. Thirunavukkarasu, R. Mohan Kumar, P.R. Umarani, J. Cryst. Growth **420** (2015) 11–16.

[6] P. Pandi, G. Peramaiyan, R. Mohan Kumar, G. Bhagavannarayana, R. Jayavel, Appl. Phys. A **112** (2013) 711-717.

[7] Tianliang Chen, Zhihua Sun, Cheng Song, Yan Ge, JunhuaLuo, Wenxiong Lin, Maochun Hong, Cryst. Growth Des. **12** (2012) 2673-2678.

[8] S. Janarthanan, R. Sugaraj Samuel, S. Selvakumar, Y.C. Rajan, D. Jayaraman and S. Pandi, J. Mater. Sci. Technol. **27** (2011) 271-274.

[9] N. Swarna Sowmya, S. Sampathkrishnan, Y. Vidyalakshmi, S. Sudhahar, R. Mohan Kumar, Spectrochim. Acta Part A **145** (2015) 333-339.

[10] D.S. Chemla, J. Zyss, Nonlinear Optical Properties of Organic molecules and crystals, 1-2, Academic Press, Orlando, New York, 1987.

[11] M. Suresh, S. Asath Bahadur and S. Athimoolam, J. Mol. Struct. **1112** (2016) 63-70.

[12] J. Mohana, G. Ahila, M. Divya Bharathi, G. Anbalagan, J. Cryst. Growth **450** (2016) 181-189.

[13] L. Jothi, K. Ramamurthi, Indian J. Sci. Technol. **4** (2011) 666-669.

[14] S. Selvakumar, A. Leo Rajesh, J. Mater. Sci. Mater. Electron. **27** (2016) 7509-7517.

[15] Kannan V, Sugumar P, Brahadeeswaran S, Ponnuswamy MN. Acta Crystallogr Sect E. **69** (2013) o610–7.

[16] G. Ganesh, A. Ramadoss, P.S. Kannan, A. SubbiahPandi, J Therm Anal Calorim. **112** (2013) 547-554

[17] Neeti Goel, Nidhi Sinha, Binay Kumar, Opt Mater. **35** (2013) 479-486.

[18] B. Babu, J. Chandrasekaran, S. Balaprabhakaran, P. Ilayabarathi Mater-Sci Poland. **31** (2013) 151-157.

[19] P. Krishnan, K. Gayathri, G. Bhagavannarayana, S. Gunasekaran, G. Anbalagan Spectrochim. Acta part A **102** (2013) 379-385.

[20] M. Prakash, D. Geetha, M. Lydia Caroline, Spectrochim. Acta part A**107** (2013) 16-23.

[21] B. Babu, J. Chandrasekaran, S. Balaprabhakaran and P. Ilayabarathi, Mater. Sci.-Pol. **31** (2013) 151-157.

[22] Mansoor Sheik-Bahae, Ali A. Said, Tai-Huei Wei, David J. Hagan, E.W. Van Stryland, IEEE J. Quantum Electron. **26** (1990) 760.

[23] E.D. D'silva, G.K. Podagatlapalli, S.V. Rao, S.M. Dharmaprakash, Mater. Res. Bull. **47** (2012) 3552.